International Tables for Crystallography (2006). Vol. C, Section 2.3.1.1.4, pp. 47–48.

essential that the setting of the worm against the gear wheel be adjusted for smooth operation. In practice, this is a compromise between minimum backlash and jerky movement. The backlash can be avoided by scanning in the same direction and running the diffractometer beyond the starting angle before beginning the data collection. Incremental angle encoders have been used when very high precision is required.

The 0° position of the diffractometer scale, $2\theta_0$, can be determined with a pinhole placed in the specimen post as shown in Fig. 2.3.1.6(*a*) (Parrish & Lowitzsch, 1959). The receiving slit is step scanned in 0.01° or smaller increments and the midpoints of chords at various heights are used to determine the angle. To avoid mis-centring errors of the pin-hole, two measurements are made with the specimen post rotated 180° between measurements. The median angle of the two plots is the 0° position as shown in Fig. 2.3.1.6(*b*) and the diffractometer scale is then reset to this position. The shape of the curves is determined by the relative sizes of the pinhole and the receiving-slit width. With care, the position can be located to about 0.001°. The $2\theta_0$ position can be corrected by using it as a variable in the least-squares refinement of the lattice parameter of a standard specimen.

Another method measures the peak angles of a number of reflections on both sides of 0°, which is equivalent to measuring 4θ. This method may be mechanically impossible with some diffractometers.

The θ–2θ setting of the specimen post is made with the diffractometer locked in the predetermined 0° position and manually (or with a stepping motor) rotating the post to the maximum intensity. A flat plate can be used as illustrated in Fig. 2.3.1.7(*a*). The setting can be made to a small fraction of a degree. Fig. 2.3.1.7(*b*) shows the effect of incorrect θ–2θ setting, which combines with the flat-specimen aberration to cause a marked broadening and decrease of peak height but no apparent shift in peak position (Parrish, 1958). The effect increases with decreasing θ and could cause systematic errors in the peak intensities as well as incorrect profile broadening.

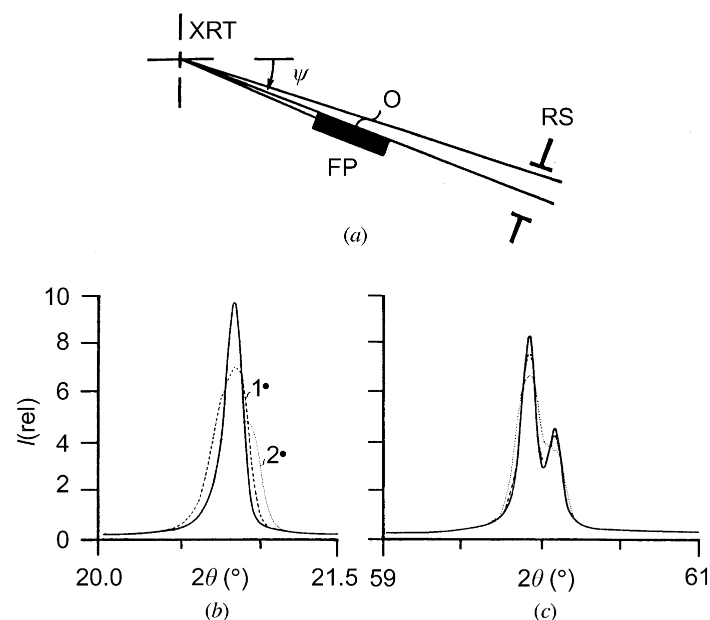

Fig. 2.3.1.7. (*a*) θ–2θ setting at 0°. Flat plate or long narrow slit is rotated to position of highest intensity. (*b*) and (*c*) Profiles obtained with correct θ–2θ setting (solid profile) and 1 and 2° mis-settings (dashed profiles) at (*b*) 21° and (*c*) 60° (2θ).

2.3.1.1.4. *Instrument broadening and aberrations*

The asymmetric form, broadening and angular shifts of the recorded profiles arise from the $K\alpha$ doublet and geometrical aberrations inherent in the imperfect focusing of the particular diffractometer method used. There are additional causes of distortions such as the time constant and scanning speed in rate-meter strip-chart recording, small crystallite size, strain, disorder stacking and similar properties of the specimen, and very small effects due to refractive index and related physical aberrations.

Perfect focusing in the sense of reflection from a mirror is never realized in powder diffractometry. The focusing is approximate (sometimes called 'parafocusing') and the practical selection of the instrument geometry and slit sizes is a compromise between intensity, resolution, and profile shape. Increasing the resolution causes a loss of intensity. When setting up a diffractometer, the effects of the various instrument and specimen factors should be taken into account as well as the required precision of the results so that they can be matched. There is no advantage in using high resolution, which increases the recording time (because of the lower intensity and smaller step increments), if the analysis does not require it. A set of runs to determine the best experimental conditions using the following descriptions as a guide should be helpful in obtaining the most useful results.

In the symmetrical geometries where the incident and reflected beams make the same angle with the specimen surface, the effect of absorption on the intensity is independent of the θ angle. This is an important advantage since the relative intensities can be compared directly without corrections. The actual intensities depend on the type of specimen. For a solid block of the material, or a compacted powder specimen, the intensity is proportional to μ^{-1}, where μ is the linear absorption coefficient of the material. The transparency aberration [equation (2.3.1.13)], however, depends on the effective absorption coefficient of the composite specimen.

The need to correct the experimental data for the various aberrations depends on the nature of the required analysis. For example, simple phase identifications can often be made using data in which the uncertainty of the lattice spacing $\Delta d/d$ is of the order of 1/1000, corresponding to about 0.025 to 0.05° precision in the useful identification range. This is readily attainable in routine practice if care is taken to minimize specimen displacement and the zero-angle calibration is properly carried out. The experimental data can then be used directly for peak search (Subsection 2.3.3.7) to determine the peak angles and intensities (Subsection 2.3.3.5) and the data entered in the search/match program for phase identification.

However, in many of the more advanced aspects of powder diffraction, as in crystal-structure determination and the characterization of materials for solid-state studies, much more detailed and more precise data are required, and this involves attention to the profile shapes. The following sections describe the origin of the instrumental factors that contribute to the shapes and shift the peaks from their correct positions. Many of these factors can be handled individually. With the use of computer programs, they can be determined collectively by using a standard sample without profile broadening and profile-fitting methods to determine the shapes (Subsection 2.3.3.6). The resulting instrument function can then be stored and used to determine the contribution of the specimen to the observed profiles.

A series of papers describing the geometrical and physical aberrations occurring in powder diffractometry has been

Copyright © 2006 International Union of Crystallography

published by Wilson (1963, 1974). His work provides the mathematical foundation for understanding the origin and treatment of the various sources of errors. The major aberrations are described in the following and are illustrated with experimental profiles and plots of computed data for better visualization and interpretation of the effects. The information can be used to correct the experimental data, interpret the profile broadening and shifts, and evaluate the precision of the analysis. Chapter 5.2 contains tables listing the centroid displacements and variances of the various aberrations.

The magnitudes of the aberrations and their effects are illustrated in Figs. 2.3.1.8(*a*) and (*b*), which show the Cu $K\alpha_1, K\alpha_2$ spectrum inside the experimental profile. At high 2θ's, the shape of the experimental profile is largely determined by the spectral distribution, but at low 2θ's the aberrations are the principal contributors. The basic experimental high-resolution profile shapes from specimens without appreciable broadening effects (NIST silicon powder standard) are shown in Figs. 2.3.1.8(*c*)–(*f*). The solid-line profiles were obtained with a reflection specimen (Fig. 2.3.1.3), and the dashed-line profiles with transmission-specimen geometry (Fig. 2.3.1.12). The differences in the $K\alpha_1, K\alpha_2$ doublet separations are explained in Subsection 2.3.1.2. These profiles are the basic instrument functions which show the profile shapes contained in all

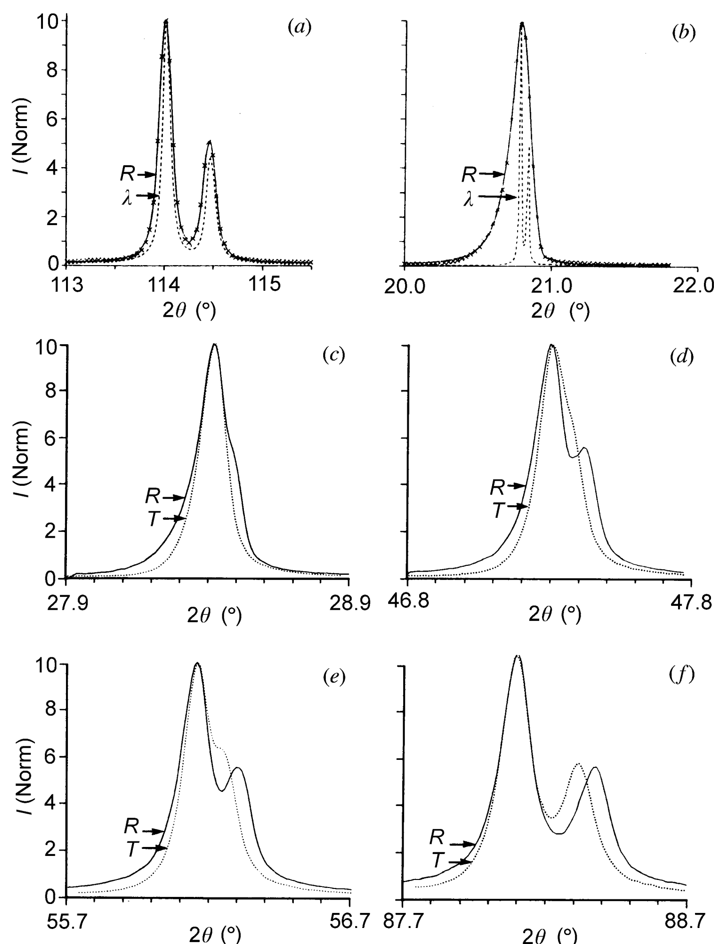

Fig. 2.3.1.8. Diffractometer profiles. (*a*) and (*b*) Spectral profiles λ of Cu $K\alpha$ doublet (dashed-line profiles) inside experimental profiles R (solid line). (*c*)–(*f*) Experimental profiles with reflection specimen (R) geometry (Fig. 2.3.1.3) with $\alpha_{\rm ES}$ 1° and $\alpha_{\rm RS}$ 0.046° (solid line profiles), and transmission specimen (T) (Fig. 2.3.1.12) with $\alpha_{\rm ES}$ 2° and receiving axial divergence parallel slits (dotted profiles). Cu $K\alpha$ radiation. (*a*) Si(531), (*b*) quartz(100), (*c*) Si(111), (*d*) Si(220), (*e*) Si(311), and (*f*) Si(422).

reflections recorded with these methods. The shapes are modified by changing slit sizes.

2.3.1.1.5. *Focal line and receiving-slit widths*

The projected source width F_w and receiving-slit width RS_w each add a symmetrical broadening to the profiles that is constant for all angles. Both the profile width and the intensity increase with increasing take-off angle (Section 2.3.5). However, the contribution of F_w is small when the line focus is used, Fig. 2.3.1.9(*a*). The receiving slit can easily be changed and it is one of the most important elements in controlling the profile width, intensity, and peak-to-background ratio, as is shown in Figs. 2.3.1.9(*a*) and (*c*). Because of the contributions of other broadening factors, $\alpha_{\rm RS}$ can be about twice α_F (line focus) without significant loss of resolution.

The projected width of the X-ray tube focus F_w is given in equation (2.3.1.2). The aperture is

$$\alpha_F = 2\arctan(F_w/2R). \tag{2.3.1.8}$$

For a line focus with actual width $F'_w = 1\,\mathrm{mm}$, $\psi = 5°$, and $R = 185\,\mathrm{mm}$, $\alpha_F = 0.011°$. The receiving-slit aperture is

$$\alpha_{\rm RS} = 2\arctan(\mathrm{RS}_w/2R). \tag{2.3.1.9}$$

For $\mathrm{RS}_w = 0.2\,\mathrm{mm}$ and $R = 185\,\mathrm{mm}$. $\alpha_{\rm RS}$ is 0.062°. The FWHM of the profiles is always greater than the receiving-slit aperture because of the other broadening factors.

2.3.1.1.6. *Aberrations related to the specimen*

The major displacement errors arising from the specimen are (1) displacement of the specimen surface from the axis of rotation, (2) use of a flat rather than a curved specimen, and (3) specimen transparency. These are illustrated schematically for the focusing plane in Fig. 2.3.1.10(*a*). The rays from a highly absorbing or very thin specimen with the same curvature as the focusing circle converge at A without broadening and at the correct 2θ. The rays from the flat surface cause an asymmetric profile shifted to B. Penetration of the beam below the surface combined with the flat specimen causes additional broadening and a shift to C.

The most frequent and usually the largest source of angular errors arises from displacement of the specimen surface from the diffractometer axis of rotation. It is not easy to avoid and may arise from several sources. It is advisable to check the reproducibility of inserting the specimen in the diffractometer by recording an isolated peak at low 2θ for each insertion. If only a radial displacement s occurs, the reflection is shifted

$$\Delta 2\theta(\mathrm{rad}) = \pm 2s\cos\theta/R, \tag{2.3.1.10}$$

where R is the diffractometer radius. A plot of equation (2.3.1.10) is shown in Fig. 2.3.1.10(*b*). The shift is to larger or smaller angles depending on the direction of the displacement and there is no broadening if the displacement is only radial and relatively small. Even a small displacement causes a relatively large shift; for example, if $s = +0.1\,\mathrm{mm}$ and $R = 185\,\mathrm{mm}$, $\Delta 2\theta = +0.06°$ at $20°2\theta$. This gives rise to a systematic error in the recorded reflection angles, which increases with decreasing 2θ. It could be handled with a $\cos\theta\cot\theta$ plot, providing it was the only source of error. There are other possible sources of displacement such as (*a*) if the bearing surface of the specimen post was not machined to lie exactly on the axis of rotation, (*b*) improper specimen preparation or insertion in which the surface was not exactly coincident with the bearing surface or (*c*) nonplanar specimen surface, irregularities, large particle sizes, and specimen transparency. Source (*a*) leads to a constant error

references